

pubs.acs.org/molecularpharmaceutics Article

# Reversible Self-Association in Lactate Dehydrogenase during Freeze-Thaw in Buffered Solutions Using Neutron Scattering

Jayesh Sonje, Seema Thakral, Susan Krueger,\* and Raj Suryanarayanan\*



**Cite This:** *Mol. Pharmaceutics* 2021, 18, 4459–4474



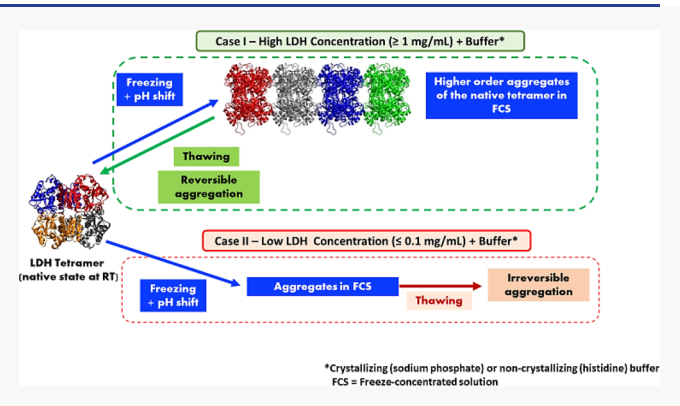
**ACCESS** 

Metrics & More

Article Recommendations

s Supporting Information

ABSTRACT: The aims of this work were to evaluate the effect of freezing and thawing stresses on lactate dehydrogenase (LDH) stability under three conditions. (i) In a solution buffered with sodium phosphate (NaP; 10 and 100 mM). The selective crystallization of disodium hydrogen phosphate during freezing caused a pronounced pH shift. (ii) In a solution buffered with histidine, where there was no pH shift due to buffer salt crystallization. (iii) At different concentrations of LDH so as to determine the self-stabilizing ability of LDH. The change in LDH tetrameric conformation was measured by small-angle neutron scattering (SANS). The pH of the phosphate buffer solutions was monitored as a function of temperature to quantify the pH shift. The conditions of buffer component crystallization from solution



were identified using low-temperature X-ray diffractometry. Dynamic light scattering (DLS) enabled us to determine the effect of freeze-thawing on the protein aggregation behavior. LDH, at a high concentration (1000  $\mu$ g/mL; buffer concentration 10 mM), has a pronounced self-stabilizing effect and did not aggregate after five freeze—thaw cycles. At lower LDH concentrations (10 and 100  $\mu$ g/mL), only with the selection of an appropriate buffer, irreversible aggregation could be avoided. While SANS provided qualitative information with respect to protein conformation, the insights from DLS were quantitative with respect to the particle size of the aggregates. SANS is the only technique which can characterize the protein both in the frozen and thawed states.

**KEYWORDS:** pH shift, LDH conformation, aggregation, sodium phosphate buffer, small-angle neutron scattering, dynamic light scattering, self-stabilization

## ■ INTRODUCTION

Protein biotherapeutics have gained significant attention in recent years. Numerous proteins (drug substances) are stored in the frozen state, sometimes for prolonged time periods, before they are formulated as solutions or freeze-dried drug products. The unique three-dimensional structure, known as the native, is responsible for the biological activity of proteins. The native structure is a result of the overall noncovalent interactions which include electrostatic and hydrophobic interactions, hydrogen bonding, and van der Waals forces. In addition to the inter- and intramolecular interactions, the stability of the native structure in solution is also influenced by the conformational entropy and external factors such as temperature, pH, protein concentration, and the presence of excipients. The protein concentration is also influenced by the conformational entropy and external factors such as temperature, pH, protein concentration, and the presence of excipients.

The stresses encountered during both freezing and freezedrying can destabilize the protein. Our current discussion will be restricted to protein destabilization in frozen systems. Several excipients can aid in stabilizing the protein and retain it in the native state. These include sugars, buffers, and surfactants, each with an intended role (functionality) in the formulation. Sugars (e.g., trehalose and sucrose) play a major role in stabilizing protein formulations. In order to exert their function, they have to be retained amorphous and resist crystallization.<sup>3</sup> The aggregation on long-term frozen storage of a monoclonal antibody formulation was attributed to crystallization of trehalose.<sup>4</sup> Selective crystallization of buffer components is also known to cause pH shifts. Many studies have indirectly shown that the pH change can be detrimental to protein stability.<sup>5–9</sup>

During the freezing process, cooling of an aqueous solution results in ice crystallization leading to concentration of excipients and protein. While some of the excipients may also crystallize, most excipients and the active ingredient (protein) remain amorphous. Thus, ice crystallization leads to, among other things, a pronounced increase in ionic strength and viscosity. The ice crystallization and cryo-concentration

Received: August 26, 2021 Revised: October 13, 2021 Accepted: October 14, 2021 Published: October 28, 2021





induce stresses which can lead to protein aggregation. 6,10 Additionally, there is a large body of evidence suggesting loss in protein activity due to its adsorption at the hydrophobic interfaces generated at the ice-water and ice-air interfaces. In most investigations, the protein stability (specifically aggregation and activity) was evaluated before and after one or multiple (up to five) freeze-thaw cycles. Similar studies have also been conducted after the entire freeze-drying cycle by reconstituting the lyophile. Due to the limitations, both in analytical techniques and in molecular modeling, the stresses experienced by the proteins during cryo-concentration have not been thoroughly studied. However, in certain cases, molecular dynamic simulation and design of experimental approaches can aid in estimating the degree of protein saturation in the freeze concentrate, gain insights into the mechanism of unfolding and aggregation at the ice-air or icefreeze concentrate interface, and determine the optimum freezing rates which will result in maximum protein stability during the freeze-thawing processes. 10,12

Among the numerous potential degradation pathways, aggregation is one of the most well-known and highly studied phenomena which can occur in diverse protein modalities differing with respect to their conformations and molecular size. Non-native aggregation, conventionally referred to as aggregation, is the formation of oligomeric units as a result of the interactions either due to conformational changes or chemical modifications in the monomeric unit. Non-native irreversible aggregates have been extensively investigated and thoroughly characterized due to the risks they pose, such as loss of efficacy and immunogenicity in protein biotherapeutics. However, a well-known but less-studied behavior observed in many enzymes and some protein modalities is native and reversible aggregation. These reversible aggregates can be attributed to noncovalent interactions between the "native" protein structures by a phenomenon referred to as "reversible self-association".13

In order to evaluate destabilization during freezing, the conventional approach is to freeze-thaw the protein solution and to characterize the analyte in the thawed solution. Our interest was to characterize the influence of excipients on the native protein conformation during the freezing and thawing processes. Small-angle neutron scattering (SANS) is an ideal technique for this purpose. It can provide information with respect to the size (on a length scale of 1 to 100 nm) and conformation of proteins in solution, when frozen and in the dried state. 14 In contrast to X-rays, neutrons are sensitive to light elements such as carbon, hydrogen, nitrogen, and oxygen, which are the building blocks of proteins. They can differentiate between isotopes of many elements, especially hydrogen. The advantages offered by neutron scattering make it a suitable technique to characterize proteins. 14-16 SANS has been used to study protein-protein interactions in two highconcentration monoclonal antibody (mAb) formulations. The higher viscosity of the mAb1 formulation was attributed to attractive protein-protein interactions, whereas charge repulsion dominated in the case of mAb2, resulting in a lower viscosity.<sup>17</sup> SANS was also used to study protein (lysozyme) crowding in the presence of sorbitol. Sorbitol was effective in reducing protein crowding in solution and in the freezeconcentrated states, thus protecting the protein from forming irreversible aggregates. 16 Contrast variation studies performed in lysozyme solutions containing glucose, trehalose, and sodium chloride demonstrated the power of this technique

to assess the protein structure in the frozen state. Irrespective of the starting excipient and protein concentration, a freeze concentrate of constant composition was obtained wherein the lysozyme existed in the monomeric state. A second population of large, reversible (in the absence of high salt) aggregates at the ice—water (freeze concentrate) and/or ice—air interface was also observed. <sup>15</sup>

Lactate dehydrogenase (LDH, molar mass 144 kDa), a globular enzyme with a tetrameric native state and an isoelectric point (pI) of  $\sim$ 7.2, was chosen as the model protein. It is known to be sensitive to freezing stresses, specifically at low pH (<5) values. <sup>18,19</sup> LDH has been used as a model protein in a number of studies to determine the effect of freeze-thawing (freezing rates, buffer crystallization, effect of surfactants, etc.).

When LDH solutions were prepared in phosphate buffer (sodium salt), frozen, and thawed, there was pronounced protein aggregation. The instability was attributed to the pH shift during freezing of the solutions. It is well-known that sodium phosphate (NaP) buffer solutions, when cooled, can exhibit pH shifts of up to ~4 units due to the selective crystallization of disodium hydrogen phosphate (one of the buffer components). While a pH shift during freezing appeared to be detrimental to proteins, a direct cause and effect relationship between pH shift and protein instability has not been established. This can be done by characterizing the system in the frozen state and again after thawing.

The LDH aggregation in frozen systems has also been attributed to adsorption on ice interface. As the surface area of ice increased (ice crystal size decreased), the effect was more pronounced. LDH was shown to partially unfold at the ice—freeze concentrate interface and the unfolding decreased in the presence of polysorbate 80. These observations were made on the cold stage of an infrared spectrometer. Interestingly, when LDH was frozen in the presence of sucrose, a well-known and effective cryo-protectant, its activity was retained. The sucrose concentration was selected so as to prevent ice formation at a low temperature. In the absence of ice, even when cooled to low temperatures, LDH retained its activity and did not undergo cold denaturation.

It is important to recognize that in most studies, if not all of these, the LDH concentration was <100  $\mu$ g/mL. It is questionable whether these results can be extrapolated to higher protein concentration systems. In light of the recent interest in high-concentration protein formulations, it will be useful to evaluate the effect of these stresses when the protein concentration is increased. For example, LDH solutions at concentrations ≥1 mg/mL, can be considered "high concentration", since the aggregation was reversible. In other words, the protein demonstrated self-stabilization. A similar stabilization effect was observed in certain high-concentration mAb systems.<sup>13</sup> Thus, this effect may be observed in different modalities of proteins. In frozen solutions, proteins are also known to exhibit concentration-dependent inhibition of excipient crystallization. For example, an albumin fusion protein inhibited the crystallization of mannitol, an excipient with a strong crystallization propensity.<sup>24</sup> If the buffer salt crystallization is inhibited by the protein, then the potential detrimental effects due to pH shift would be avoided.

The first set of studies was conducted in solutions buffered with histidine. With this noncrystallizing buffer ( $pK_a$  6.0), we do not expect pronounced pH shifts during freezing. Therefore, any protein destabilization could be attributed to

the stresses associated with freezing and thawing. The second set of studies was conducted with NaP buffer at two concentrations, 10 mmol and 100 mmol/L (mM). The buffer  $pK_a$  of relevance [second  $pK_a$  of ~6.8 at room temperature (RT)] is close to the isoelectric point of LDH (pI  $\sim$  7.2), rendering it ideal for use in solutions at RT. However, NaP buffer solution, when cooled, is known to exhibit a pH shift due to selective crystallization of one of the buffer components. At 100 mM buffer concentration, a detrimental effect due to pH shift was observed in the case of ribonuclease A. When a 100 mM NaP buffer with a starting pH of 6.4 was frozen from 25 to -20 °C in the presence of ribonuclease A (1.5 mg/mL), the pH decreased to 4.3 as opposed to a pH drop to 4.6 in a buffer-alone system.<sup>25</sup> Even a higher protein concentration of 10 mg/mL (BSA or  $\beta$ -galactosidase) did not significantly attenuate the pH when the NaP buffer concentration was 100 mM.7 Therefore, this buffer concentration was considered the "worst case" (negative control). Although a pH shift is observed when a 10 mM phosphate buffer is frozen, the presence of LDH, in a concentration-dependent manner, is expected to inhibit buffer crystallization and attenuate the pH shift.

The overall objective of the study was to elucidate the aggregation behavior of LDH during freezing and thawing. The specific aims of the study were to evaluate the effect of freezing stresses on LDH stability under three conditions: (i) in a solution buffered with NaP. The selective crystallization of disodium hydrogen phosphate during freezing is known to cause a pH shift. The magnitude of pH shift was altered using two different concentrations of NaP buffer (10 and 100 mM). (ii) In a solution buffered with histidine (10 mM). In this system, there will be no pH shift due to buffer salt crystallization. (iii) At different concentrations of LDH so as to determine the self-stabilizing ability of LDH. These systems were subjected to multiple freezing and thawing. The protein behavior was characterized in real-time using SANS, during freezing and thawing. Molecular modeling was used to determine the nature of the aggregates and thereby gain mechanistic insights into the aggregate reversibility.

While SANS was the predominant analytical technique, several orthogonal techniques were used. Native size and shape of LDH in NaP-buffered solutions were also determined using small-angle X-ray scattering (SAXS). The pH of the NaP buffer solutions was monitored as a function of temperature to quantify the pH shift. The low-temperature powder X-ray diffractometry (XRD) of these solutions enabled us to identify the conditions of buffer component crystallization from solution. Differential scanning calorimetry (DSC) allowed the measurement of the melting temperature of the NaP buffer solutions. Finally, dynamic light scattering (DLS) enabled us to determine the effect of freeze-thawing on the protein aggregation behavior for LDH at different concentrations in NaP and histidine buffers.

# ■ MATERIALS AND METHODS

**Materials.** LDH from rabbit muscle ( $M_{\rm w}$  = 144 kDa) was obtained from Sigma-Aldrich (St. Louis, MO) at 5 or 10 mg/mL as a suspension in 3.2 mol/L (M) ammonium sulphate (pH 6.0). Sodium phosphate heptahydrate, sodium phosphate dibasic monohydrate, L-histidine, and L-histidine monohydrochloride were purchased from Sigma-Aldrich (St. Louis, MO).

Deuterium oxide, D<sub>2</sub>O (99.9%), was purchased from Cambridge Isotope (Tewksbury, MA). Prior to SANS

measurements, the LDH was dialyzed at 4 °C into either 10 mM histidine buffer containing 8% D<sub>2</sub>O, 10 mM histidine buffer containing 100% D<sub>2</sub>O, 10 mM NaP buffer containing 8% D<sub>2</sub>O, or 100 mM NaP buffer containing 8% D<sub>2</sub>O. Before dialysis, LDH was diluted to 2 or 3 mg/mL using the dialysis buffers. The dialysis was accomplished using 20 kDa MWCO Slide-A-Lyzer mini dialysis devices (Thermo Fisher Scientific, Waltham, MA) for 0.5 to 2.0 mL volume. Buffer was exchanged after 2 h, and the samples were then left to dialyze overnight. The LDH as received was a turbid suspension, but the solution was clear following dialysis. LDH concentration was measured after dialysis using a Nanodrop spectrophotometer (Thermo Fisher Scientific, Waltham, MA) using an extinction coefficient at 280 nm of 1.9 mL/mg cm at 280 nm. Samples for SAXS measurements were prepared in 100 mM NaP buffer containing 0% D<sub>2</sub>O in a similar manner.

SANS Measurements. SANS measurements were performed on the NGB 30 m SANS instrument at the National Institute of Standards and Technology (NIST), Center for Neutron Research (NCNR) in Gaithersburg, MD.<sup>26</sup> The samples were loaded into demountable 1 mm sample path length titanium (Ti) cells with Ti windows and cooled from 20 to -45 °C at a ramping rate of 0.5 °C per minute using a closed-cycle refrigerator with a two-position sample holder. The samples were measured at 20, 5, 0, -10, -25, and -45°C. Counting times at each temperature were ~1.0 h per sample at 20 °C and 0.5 h per sample at all other temperatures, effectively holding the samples at each temperature for 1 h to make the measurements before proceeding to the next temperature. Samples were then heated back to 20 °C at the same ramping rate and measured at the same temperatures for the same times as during cooling. Empty cells were also measured in both sample positions for  $\sim$ 0.5 h at 20 °C.

A neutron wavelength of  $\lambda = 6$  Å was used with a wavelength spread  $\Delta \lambda/\lambda = 0.14$ . The scattered neutrons were detected with a 64 cm × 64 cm two-dimensional position-sensitive detector with 128 pixels × 128 pixels at a resolution of 0.5 cm/ pixel. Data reduction was performed using IGOR Pro (Wavemetrics Inc., Lake Oswego, OR) with SANS macros developed at the NCNR.<sup>27</sup> Raw counts were normalized to a common neutron intensity and corrected for empty cell counts, ambient room background, and nonuniform detector response before being placed on an absolute scale by normalizing the intensity to the incident beam flux. Finally, the data were radially averaged to produce the scattered intensity, I(q) versus q, where  $q = 4\pi \sin(\theta)/\lambda$  and  $2\theta$  is the scattering angle. Sample-to-detector distances of 13, 4.5, and 2 m were used for each measurement to obtain a q range between 0.004 and 0.3 Å<sup>-1</sup>. Scattering from the buffer was subtracted from a subset of the samples in order to compare the buffer-subtracted data with calculated SANS curves from atomic coordinates. Guinier fits were made to a subset of the buffer-subtracted data to obtain the radius of gyration,  $R_o$ , and the forward scattering intensity, I(0).

**SAXS Measurements.** Aqueous LDH solutions and buffers were filled in 1.5 mm quartz capillaries, which were sealed hermetically. SAXS measurements were performed on an SAXSLab Ganesha 300XL. Cu K $\alpha$  X-rays ( $\lambda$  = 1.54 Å) generated using a Xenocs Geni3DX source were collimated through two sets of four-bladed slits (JJ X-ray, A/S). Two-dimensional SAXS images were acquired using a Dectris EIGER R 1M detector (7.72 cm × 7.99 cm rectangular area) with 1030 pixels × 1065 pixels (75  $\mu$ m × 75  $\mu$ m pixel size) at a

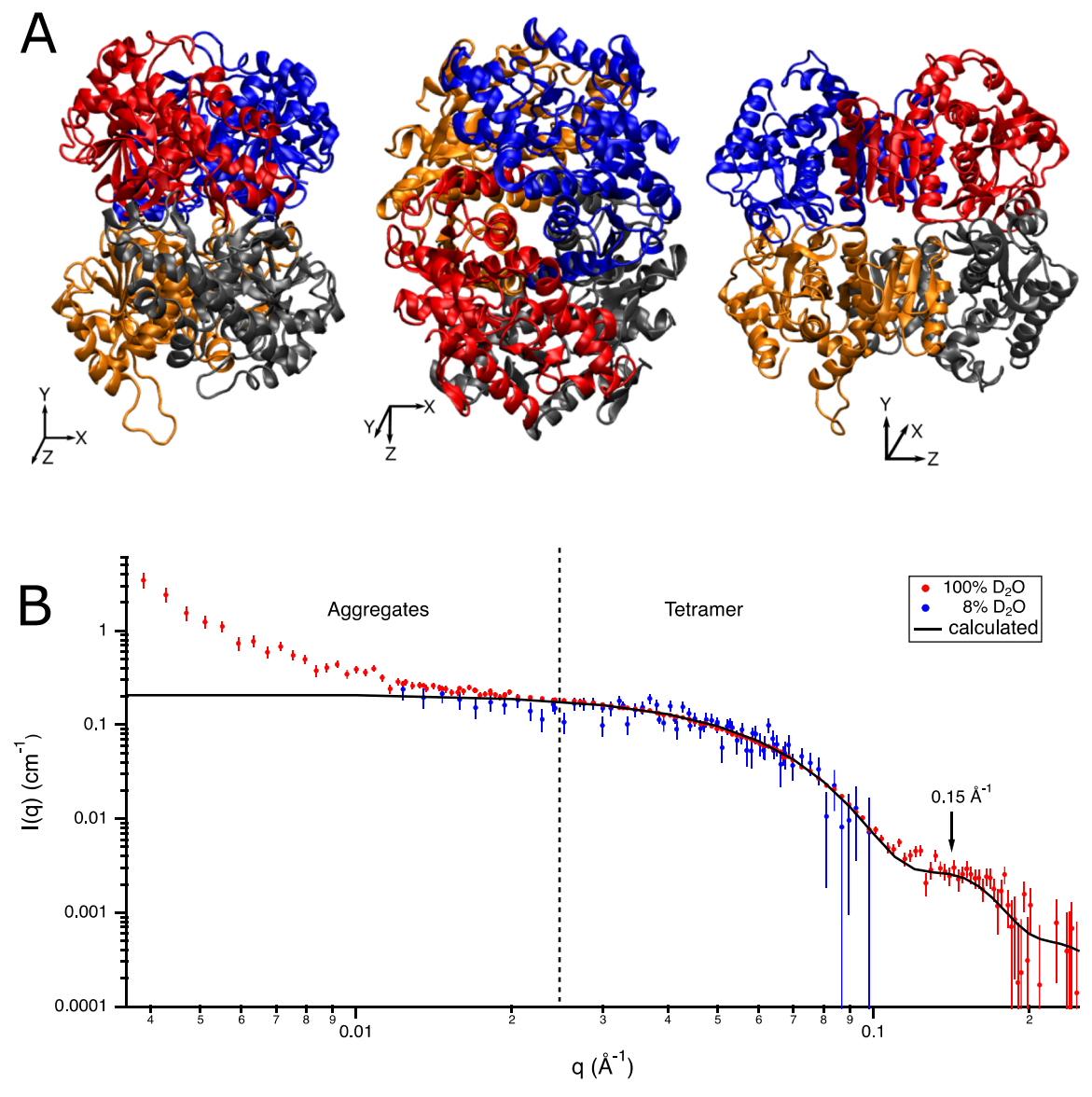


Figure 1. A) LDH tetramer (PDB ID 2V6M)<sup>28</sup> visualized in three different orientations using VMD.<sup>32</sup> (B) Overlay of buffer-subtracted SANS curves for 1 mg/mL LDH in 10 mM histidine buffer in 100%  $D_2O$  (red data points) and in 8%  $D_2O$  (blue data points) at 20 °C and the calculated LDH tetramer curve (black curve) from the structure in A using the SasCalc module in SASSIE-web.<sup>34</sup> The 8%  $D_2O$  data have been scaled to the 100%  $D_2O$  data for easy comparison of their shapes. Error bars are the standard error of the mean based on the number of pixels used during data averaging.

sample-to-detector distance of 45 cm. Each sample was measured for 2 h. SAXS images were azimuthally integrated using SAXSGUI, to obtain one-dimensional scattered intensity I(q) versus q plots. The data were placed on an absolute scale by normalizing the intensity to the incident beam flux. Background subtraction and Guinier fits were performed using IGOR Pro as described above.

LDH Structure Modeling. LDH dimers, tetramers, octamers, and 16-mers were modeled from the tetramer structure of the apo form of LDH from *Thermus thermophilus*,<sup>28</sup> Protein Data Bank identifier (PDB ID) 2V6M. Missing H atoms and residues were added to the structure using PSFGEN<sup>29</sup> to create a tetramer structure suitable for modeling using the CHARMM force field.<sup>30</sup> This structure was energy-minimized and then subjected to a 10 ps molecular dynamics (MD) simulation using NAMD<sup>29</sup> to ensure that the structure was stable. To make LDH octamers

and 16-mers, the energy-minimized and MD-subjected structure was aligned along its principle axes with its center of mass at the origin using the build utilities module in SASSIE-web. Using VMD, identical tetramers with different positions along the x, y, and z principal axes were created in order to construct three different octamers and 16-mers along these axes using only geometrical considerations. The energy-minimized and MD-subjected tetramer structure was also used to construct three dimer structures. Model SANS curves and  $R_g$  were calculated from the model structure using the SasCalc module in SASSIE-web. Expected I(0) values were calculated using the contrast calculator module in SASSIE-web.

Calculation of the Isoelectric Point and Net Charge on LDH. The isoelectric charge (pI) and the net charge (z) on the LDH amino acid sequence as a function of pH was determined using the Prot pi Peptide tool (https://www.protpi.ch/Calculator/PeptideTool). The determination was

Table 1. Basic Characterization of LDH at 20 °C before and after Freezing<sup>a</sup>

sample	LDH concentration (mg/mL)	Guinier $R_{\rm g}$ (Å)	$qR_{\rm g}$ range	Guinier $I(0)$ (cm <sup>-1</sup> )	calculated $I(0)$ (cm <sup>-1</sup> )		
		SANS (8% D <sub>2</sub> O)					
10 mM NaP	1.25	$27 \pm 2$	0.62 - 1.29	$0.057 \pm 0.002$	0.055		
10 mM NaP, 1× FT	1.25	$28 \pm 3$	0.53 - 1.29	$0.040 \pm 0.002$	0.055		
100 mM NaP	1.27	$33 \pm 3$	0.66 - 1.29	$0.063 \pm 0.004$	0.056		
100 mM NaP, 1× FT	1.27	$32 \pm 3$	0.62 - 1.29	$0.051 \pm 0.004$	0.056		
10 mM histidine	0.89	$28 \pm 3$	0.34 - 1.28	$0.041 \pm 0.002$	0.039		
10 mM histidine, 1× FT	0.89	$28 \pm 3$	0.63 - 1.28	$0.037 \pm 0.003$	0.039		
SAXS (0% D <sub>2</sub> O)							
100 mM NaP	0.6-0.7	$28 \pm 2$	0.63 - 1.28	$0.080 \pm 0.003$	0.06-0.07		
100 mM NaP, 5× FT	0.6-0.7	$28 \pm 2$	0.66 - 1.27	$0.038 \pm 0.003$	0.06 - 0.07		

<sup>&</sup>quot;Error bars on the measured concentration for the SANS samples are about 5%. Error bars on  $R_g$  and I(0) are standard errors on the slope and intercept, respectively, from the linear Guinier fit to  $\ln[I(q)]$  vs  $q^2$ . The calculated  $R_g$  from the coordinates (PDB ID 2V6M)<sup>28</sup> is 30 Å using the SasCalc module in SASSIE-web.<sup>34</sup> Calculated I(0) values were obtained using the contrast calculator module in SASSIE-web.<sup>35</sup>

performed using the known LDH structure from the Protein Data Bank (PDB ID 2V6M—the same as that used for structure modeling). The representative snapshot of the values obtained for the surface charge on LDH at a particular pH is included in the Supporting Information.

DSC of NaP Buffer Solutions. A differential scanning calorimeter (model Q2000 TA Instruments, USA) equipped with a cooling system was used to perform low-temperature thermal analysis. The instrument was periodically calibrated with indium and tin. Dry nitrogen at a flow rate of 50 mg/mL was used as purge gas. Aluminum pans, hermetically sealed with 15 to 20 mg of the sample, was weighed and cooled to -45 °C, held for 10 min to achieve equilibrium, and warmed to 20 °C at 0.5 °C/min. Due to the stochastic nature of cooling curves, the information obtained was only used for qualitative purposes. For any quantitative data interpretation, the heating curves were used.

Low-Temperature pH of NaP Buffer Solutions. The NaP buffer solutions were frozen and thawed in a jacketed beaker using a controlled temperature program. About 50 mL of sample solution was placed in a 250 mL jacketed beaker and the temperature was maintained using a circulating external water bath (NesLab RTE 740, Thermo Electron, USA). A lowtemperature pH electrode (Inlabcool, Mettler Toledo, Switzerland) was used for measurement of pH using FRISCOLYT-B as a reference solution which enables measurement of electromotive force (EMF) at temperatures up to -30 °C. The probe is placed at the center of the solution in the 250 mL beaker taking care to prevent it from touching the base of the beaker and is connected to a pH meter (pH 500 series, Singapore). The measured EMF was then used to calculate the solution pH. A copper-constantan thermocouple (Omega, USA) with Teflon insulation was connected to a benchtop digital read out device (±0.2 °C, OmegaMDSi8 Series, USA). The instrument calibration procedure and calculation of pH from EMF potential were performed based on previous literature reports. 6,36

**Low-Temperature XRD of NaP Buffer Solutions.** An X-ray diffractometer (D8 ADVANCE, Bruker AXS, USA) with a variable-temperature stage (TTK 450, Anton Paar, Austria) and Si strip one-dimensional detector (LynxEye, Bruker AXS, USA) was used. The NaP buffer sample ( $\sim$ 100  $\mu$ L) was placed in a copper XRD sample holder with a thermocouple used to record the sample temperature. The solutions were subjected to controlled temperature program, and the diffraction curves using Cu K $\alpha$  radiation (1.54 Å; 40 kV × 40 mA) were

obtained by scanning over an angular range of  $7-35^{\circ}$  ( $2\theta$ ) with a step size of  $0.05^{\circ}$ . A dwell time of 0.5 s for the 100 mM NaP buffer and 4 s for 10 mM NaP buffer was used. The samples were cooled and heated at  $0.5^{\circ}$ C/min, and scans were collected at selected time points during cooling and heating.

Dynamic Light Scattering. DLS experiments were performed to determine the LDH aggregates pre- and postfreeze—thaw in solution at RT. The hydrodynamic radius (nm) of the particles and the particle size distribution were measured using an UNCLE instrument (Unchained Labs, CA). The sample volume for individual measurements was 9  $\mu$ L. Each measurement was an average of five scans with a run time of  $\sim$ 10 s. A similar dialysis procedure to that noted above was used to prepare 1000  $\mu$ g/mL LDH solutions in 10 mM histidine and 10 and 100 mM NaP buffers, as mentioned earlier. These stock solutions were diluted to prepare 10 and 100  $\mu$ g/mL LDH solutions under the different buffer conditions. The solutions were cooled from RT to -45 °C at 0.5 °C/min, held at -45 °C for 30 min, and heated back to RT at 0.5 °C/min in a benchtop freeze-drier (VirTis, SP Scientific, PA). The procedure was repeated five times (5× FT). Samples were stored in dry ice until analyzed.

# ■ RESULTS AND DISCUSSION

Our first set of studies in histidine buffer was aimed at determining the native protein conformation of LDH and its conformations in the frozen state. These preliminary measurements enabled identification of LDH in the frozen state using different ratios of  $\rm H_2O$  to  $\rm D_2O$  in the buffer. After establishing the protein conformation, comparative studies were conducted in NaP-buffered solutions (10 and 100 mM). The analyses were carried out in the following stages: (i) immediately after preparing a solution at RT, (ii) during freezing to  $-45~\rm ^{\circ}C$ , and (iii) during thawing to RT.

**Conformation of LDH at RT.** Figure 1A shows three views of the LDH structure from PDB ID 2V6M. Figure 1B contains the buffer-subtracted SANS data from LDH (~1 mg/mL) buffered in histidine (10 mM) in 100% D<sub>2</sub>O and 8% D<sub>2</sub>O at RT before freezing. Due to its higher scattering length density and low incoherent scattering, D<sub>2</sub>O was initially used as the solvent medium for the SANS experiments. The vertical dotted line splits the data into the low q scattering region (LQS) for q < 0.025 Å<sup>-1</sup> and the high q scattering region (HQS) for q > 0.025 Å<sup>-1</sup>. While D<sub>2</sub>O was ideally suited for gaining conformational insights into the HQS, especially for q > 0.1 Å<sup>-1</sup>, the hydrophobic effect induced by deuterium

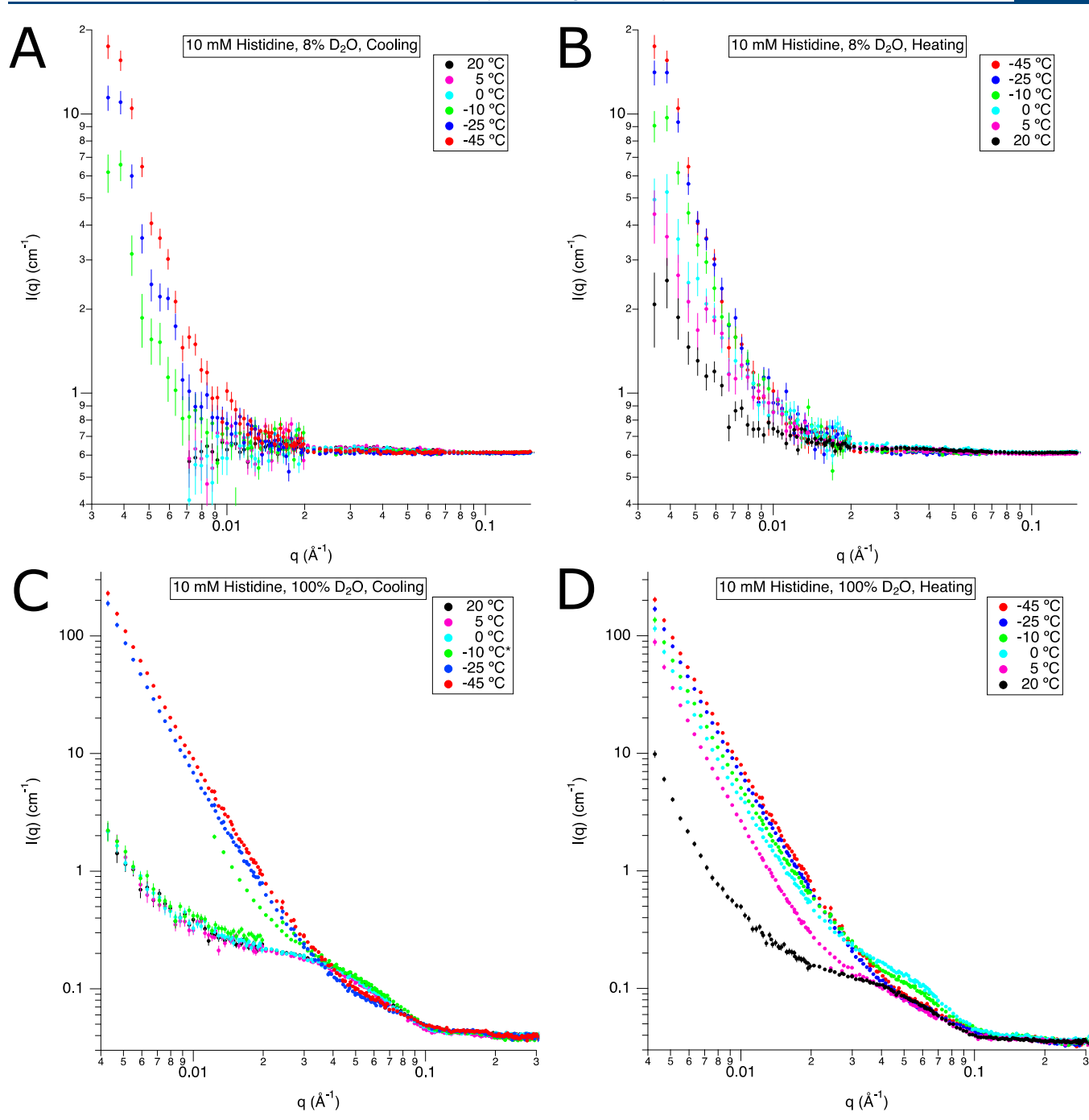


Figure 2. SANS I(q) vs q curves. (A) LDH (1 mg/mL) in 10 mM histidine buffer in 8% D<sub>2</sub>O during cooling at 20, 5, 0, -10, -25, and -45 °C from bottom to top. (B) Frozen solution (of panel A) during heating at -45, -25, -10, 0, 5, and 20 °C from top to bottom. (C,D) SANS profiles for the identical composition obtained during cooling and heating but in 100% D<sub>2</sub>O. The incoherent scattering from the buffer has not been subtracted from these data in order to show the difference in the incoherent scattering between the 8% D<sub>2</sub>O and 100% D<sub>2</sub>O buffers. Error bars are the standard error of the mean based on the number of pixels used during data averaging. \*In Figure 1C, the SANS pattern at -10 °C does not align in the 0.01 to 0.03 Å<sup>-1</sup> range; this discontinuity can be attributed to the beginning of ice crystallization or incomplete ice crystallization at -10 °C.

promoted aggregation in the solution immediately after dialysis, which is evident in the LQS. Moreover, the protein signal was compromised on freezing due to the pronounced scattering from the ice—air interface, as was shown in Curtis et al.<sup>15</sup> The contrast match point of 8% D<sub>2</sub>O and 92% H<sub>2</sub>O, where the ice—air scattering became invisible, was also established in that work. Thus, contrast variation measurements under these conditions enabled us to determine the

structure of LDH in the frozen state without interference from the scattering at the ice—air interface.

The model SANS curve calculated as described in the Materials and Methods section is shown as the solid black line in Figure 1B. It predicts the solution scattering of the structure in Figure 1A averaged over all possible orientations. There is little difference between the model SANS curves calculated for LDH in 8% D<sub>2</sub>O and 100% D<sub>2</sub>O buffers. It is important to note that the scattering from the modeled LDH tetramer

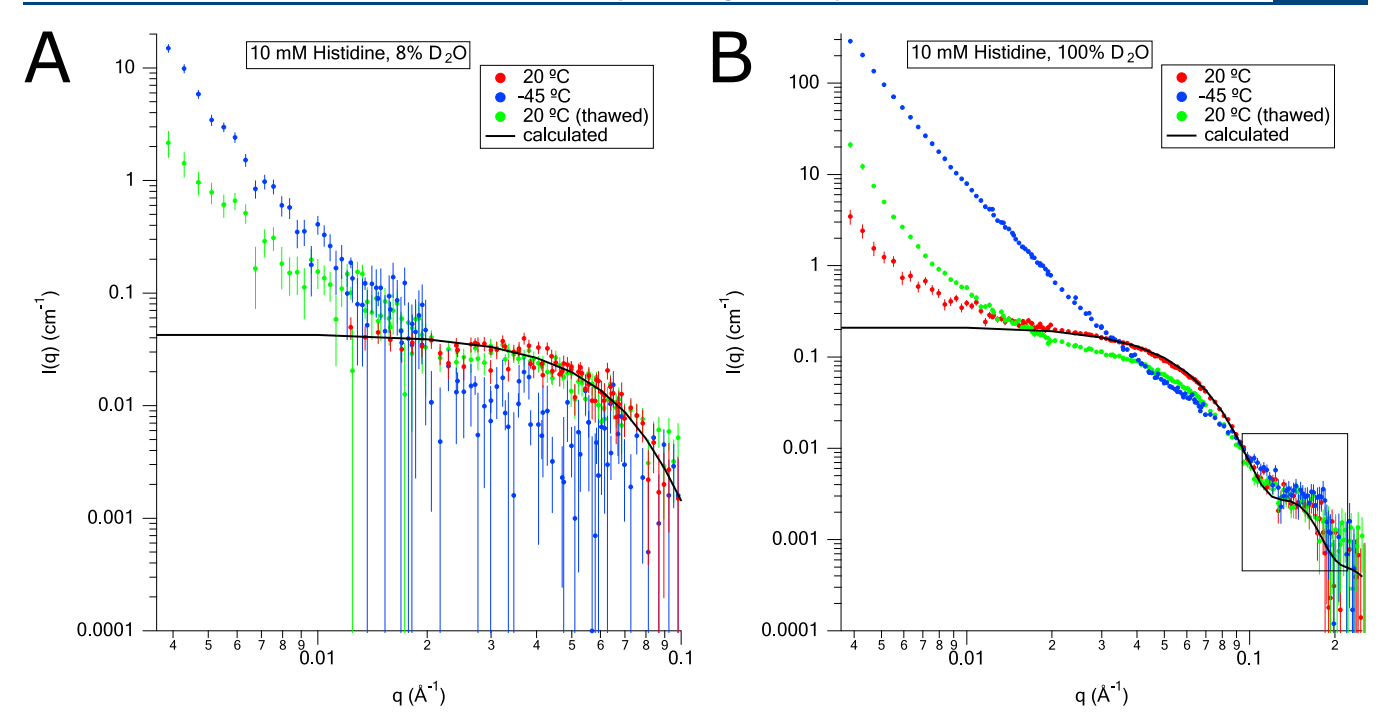


Figure 3. SANS I(q) vs q curves. (A) Buffer-subtracted SANS curves of LDH (1 mg/mL) solution buffered in histidine (10 mM; 8% D<sub>2</sub>O) at RT (red circle), cooled to -45 °C (blue circle) and thawed back to RT (green circle). The black curve is the reference LDH tetramer curve. (B) Same composition and processing conditions as in panel (A), except for the use of 100% D<sub>2</sub>O. Error bars are the standard error of the mean based on the number of pixels used during data averaging.

shows two characteristic features: (i) a flat shape in the LQS region which is expected due to the absence of large structures or aggregates and is also an indication of monodispersed solution and (ii) two features in the HQS region from 0.03 to 0.1  $\text{Å}^{-1}$  and one at  $\sim$ 0.15  $\text{Å}^{-1}$ .

The calculated SANS curve matched the data in 8% D<sub>2</sub>O buffer very well, confirming the existence of LDH as a tetramer at RT in 10 mM histidine buffer. Although the data in 100% D<sub>2</sub>O showed aggregation in the LQS, they matched the calculated SANS curve very well in the HQS, including the subsidiary maximum at  $q \sim 0.15 \text{ Å}^{-1}$ , suggesting that there is still a significant population of tetramers in 100% D<sub>2</sub>O buffer. We also confirmed the tetrameric state of LDH by comparing the Guinier-derived  $R_{\sigma}$  and I(0) values from the 8%  $D_2O$  data to those calculated from the LDH tetramer structure. The results are shown in Table 1. Virtually identical results were obtained from LDH in 8% D<sub>2</sub>O 10 and 100 mM NaP buffers, as shown in Table 1. Guinier fits to SAXS data obtained from LDH in 0% D<sub>2</sub>O 100 mM NaP buffer further confirmed the existence of the tetramer in solution at RT, and these results are also included in Table 1. The lower I(0) values after thawing could be due to the loss of the sample from the formation of air bubbles that remain after thawing, resulting in less sample in the beam. The SAXS data, as well as the Guinier plots from the SANS and SAXS data, are presented in the Supporting Information as Figures S1–S4.

Freeze-Thaw of LDH in Histidine Buffer. The next objective was to determine the effect of freeze-thawing on LDH conformation. We will first discuss the results from freeze-thawing LDH in 10 mM histidine buffer. The samples were cooled to -45 °C at 0.5 °C/min, held for 2 h, and then heated back to 20 °C at the same rate. SANS curves were collected at different temperatures during freezing and thawing. During cooling to 5 °C in 8% D<sub>2</sub>O buffer (Figure 2A), there

was no change in the LQS, suggesting the retention of the protein in the native state. As it was further cooled from 0 to  $-45\,^{\circ}\text{C}$ , we see a dramatic increase in LQS intensity at  $-10\,^{\circ}\text{C}$ , indicative of LDH aggregation when the sample froze, followed by a more gradual increase as the temperature is decreased further. Recall that the scattering from the ice—air interface is absent in 8% D<sub>2</sub>O buffer and we can thus attribute the measured intensity entirely to LDH aggregates.

Cooling the buffer solution resulted in ice crystallization leading to buffer component (histidine) freeze concentration. At the concentration used (10 mM, pH 6.0), the buffer remains amorphous. The decrease in temperature will influence the p $K_a$  of histidine. This dp $K_a/dT$  has been calculated to be  $-0.022~K^{-1}$ . In 20 mM L-histidine buffer solution, the pH increased from 5.37 to 6.14 when the temperature was decreased from 25 to  $-30~^{\circ}C$ . It is instructive to recognize that our buffer concentration was lower (10 mM) and the pH of our buffer solution at RT was 6.0 (close to the p $K_{a2}$  of histidine at RT). Thus, while the decrease in temperature and the attendant freeze concentration would bring about a small change in the pH, we do not know the magnitude of this effect in the presence of LDH.

The LDH aggregation that was observed in the frozen solution could be attributed to charge—charge interactions. When the pH of the solution is 6.0 units, the calculated net positive charge on LDH was 10 units (Figure S5). Thus, the aggregation could have been brought about by the high net positive surface charge on LDH. <sup>13,39</sup> Close packing of these positively charged LDH molecules can result in charge—charge repulsion resulting in expansion or modification of the tetramer conformation to accommodate the charge which in turn can facilitate favorable long-range Coulombic interactions. These long-range Coulombic attractions may lead to the formation of higher-order aggregates in the freeze concen-

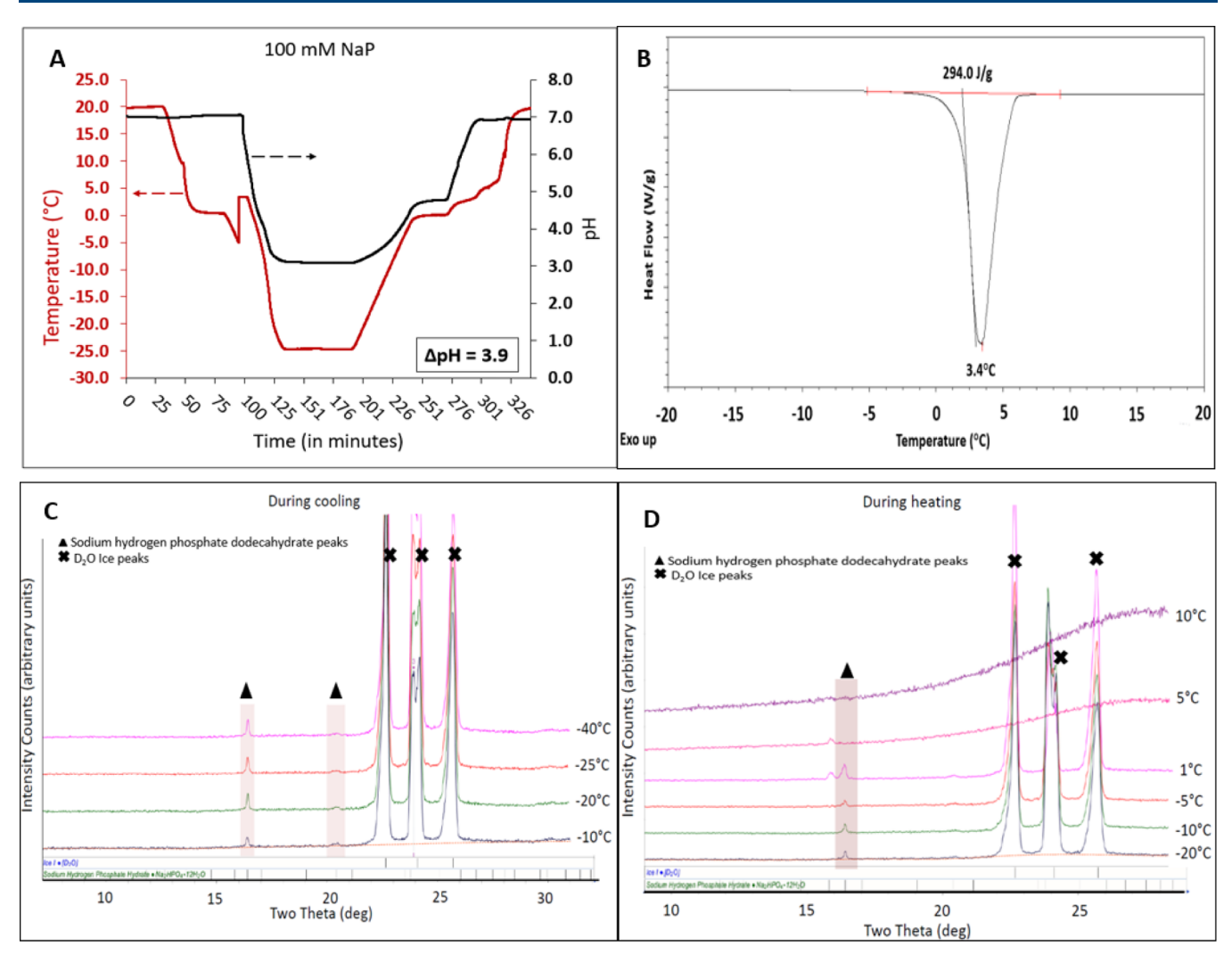


Figure 4. Characterization of NaP buffer (100 mM) during freezing and thawing (in 100%  $D_2O$ ). (A) Low-temperature pH measurement, when cooled from 20 to  $-25\,^{\circ}$ C and then heated back to 20  $^{\circ}$ C. The heating and cooling rate was 0.5  $^{\circ}$ C/min, and the frozen solution was held at  $-25\,^{\circ}$ C for 30 min. (B) DSC heating curve of frozen solution, heated from -45 to 20  $^{\circ}$ C. The solution was initially cooled from RT to  $-45\,^{\circ}$ C, at 0.5  $^{\circ}$ C/min, and held for 30 min. Only the final heating curve is shown. (C) XRD patterns obtained while the solution was cooled from 20 to  $-40\,^{\circ}$ C at 0.5  $^{\circ}$ C/min. The XRD patterns were obtained at -10, -20, 25, and  $-40\,^{\circ}$ C. (D) XRD patterns obtained when the frozen solution (from C) was heated from  $-40\,^{\circ}$ C at 0.5  $^{\circ}$ C/min. The XRD patterns were obtained at -20, -10, -5, 1, 5, and 10  $^{\circ}$ C.

trate. 13,39-41 In addition, aggregation brought about by interaction at the ice-water and/or ice-air interfaces cannot be ruled out

During warming of the frozen solution (Figure 2B), from -45 to 0 °C, the aggregation persisted and the ice melting was not complete. Even when the ice melting was complete at 5 °C, the aggregates persisted. By 20 °C, there is still some scattering in the LQS, compared to none before freezing, indicating that some aggregates were retained upon thawing from -45 °C. Thus, aggregation was predominantly reversible and a fraction of the sample possibly undergoes irreversible aggregation. Another possible explanation is that at 1000  $\mu$ g/mL LDH concentration, the aggregation is reversible, but it was not complete at the time we measured the sample, that is, immediately after thawing.

Similar SANS curves were obtained in 100%  $D_2O$  10 mM histidine buffer (Figure 2C,D). However, due to the lower incoherent background, more detail can be observed in the HQS. Figure 2C shows that freezing occurred at  $-10\,^{\circ}$ C, where in fact, we see a discontinuous SANS intensity (green

curve) since the sample froze after the LQS scattering had been measured. Upon freezing, we see that the scattering in the LQS increases and that the scattering curve in the HQS between q=0.025 and  $0.1~{\rm \AA}^{-1}$  decreases as well as changes in shape, indicating that the population shifts from mostly tetrameric molecules to higher-order aggregates as the freezing progresses. The LQS scattering is higher than that observed in 8% D<sub>2</sub>O due to the added contribution from the ice—air interface that is absent in the 8% D<sub>2</sub>O data. Figure 2D shows that the sample thawed between 5 and 20 °C and that the aggregation at RT was higher after thawing, as observed in the 8% D<sub>2</sub>O sample.

The buffer-subtracted data for LDH in 8%  $D_2O$  and 100%  $D_2O$  10 mM histidine buffers at RT, before and after freezing, and at -45 °C are shown in Figure 3 along with the calculated SANS curve. At RT, the calculated scattering curve matched the measured scattering curve well in both the LQS and HQS for the 8%  $D_2O$  data and in the HQS for the 100%  $D_2O$  data, as already shown in Figure 1. Upon cooling to -45 °C, a pronounced deviation from the native structure is evident for

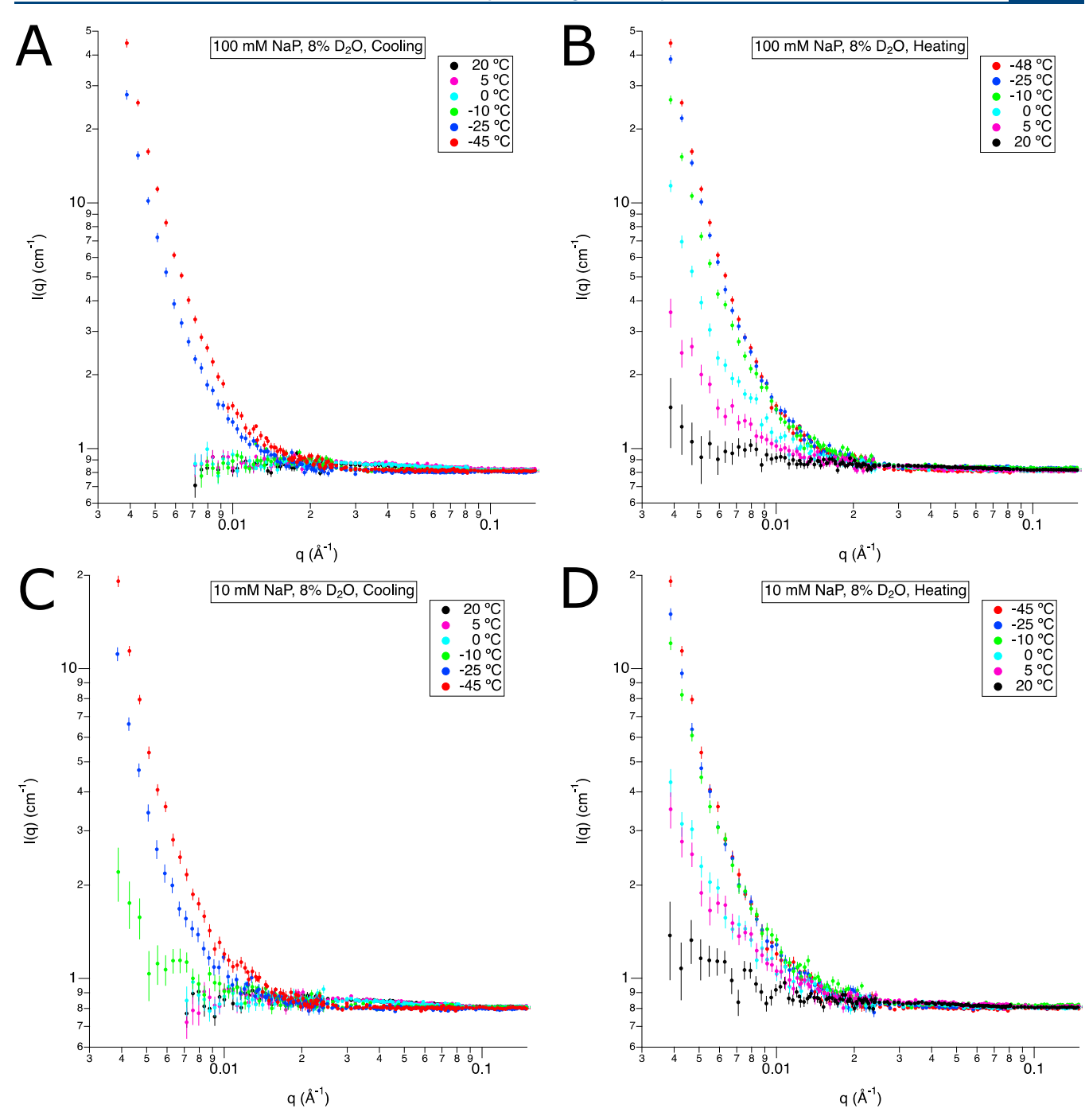


Figure 5. SANS I(q) vs q curves. (A) 1 mg/mL LDH, 100 mM sodium phosphate (NaP) 8% D<sub>2</sub>O buffer during cooling at 20, 5, 0, -10, -25, and -45 °C from bottom to top and (B) 1 mg/mL LDH, 100 mM NaP 8% D<sub>2</sub>O buffer during heating at -45, -25, -10, 0, 5, and 20 °C from top to bottom. (C,D) SANS profiles for 1 mg/mL LDH, 10 mM NaP 8% D<sub>2</sub>O buffer during identical cooling and heating series. The incoherent scattering from the buffer has not been subtracted from these data for comparison to the data in Figure 2A,B. Error bars are the standard error of the mean based on the number of pixels used during data averaging.

the LQS scattering in both buffers and a loss of the tetramer signal is seen in the HQS between q=0.025 and  $0.1~{\rm \AA}^{-1}$ . However, there is still some evidence of the subsidiary maximum from the tetrameric structure at  $q=0.15~{\rm \AA}^{-1}$  in 100% D<sub>2</sub>O buffer (Figure 3B, region in box). This shows that the aggregates that form in the frozen state likely assemble from the tetramer. Thus, the native tetrameric structure is not lost upon freezing but rather becomes the building block for the higher-order aggregates.

On thawing back to 20 °C, the pre- and post-freeze—thaw SANS curves (LQS < 0.01 Å $^{-1}$ ) at 20 °C did not overlap, revealing the existence of additional higher-order structures. The use of 100%  $\rm D_2O$  enabled the confirmation of the tetramer as the building block for the aggregates upon freezing since the lower incoherent scattering allowed the subsidiary maximum at q=0.15 Å $^{-1}$  to be observed and tracked throughout the freeze—thaw process. The SANS curves obtained, both during freezing and post-thawing, confirmed the existence of higher-order structures upon freezing. Since

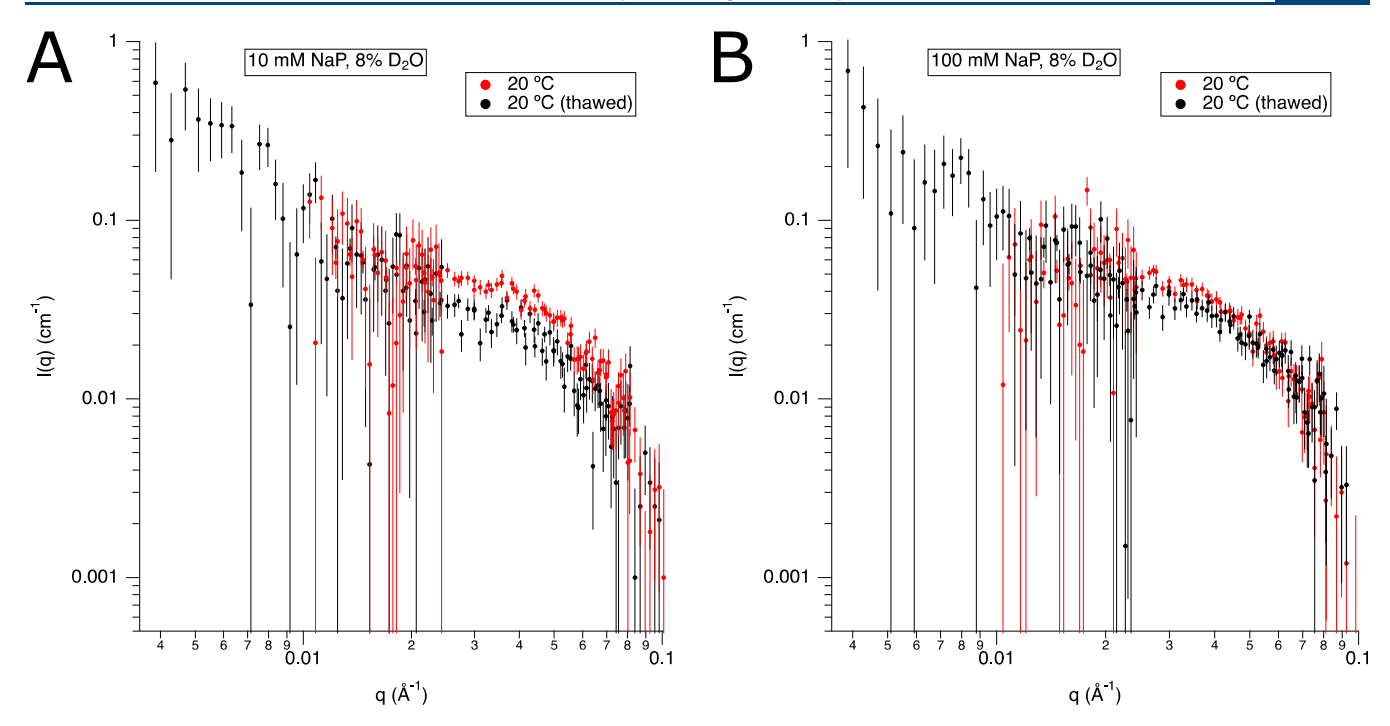


Figure 6. Overlay of buffer-subtracted SANS I(q) vs q curves pre- and post-freeze—thaw for 1 mg/mL LDH in (A) 10 mM NaP and (B) 100 mM NaP buffers in 8% D<sub>2</sub>O. Error bars are the standard error of the mean based on the number of pixels used during data averaging.

the 100%  $D_2O$  curves also contain a contribution from the air—ice interface, the 8%  $D_2O$  curves were needed in order to confirm that the LDH was, in fact, forming higher-order structures upon freezing. Thus, the two freeze—thaw sets of SANS data in 8%  $D_2O$  and 100%  $D_2O$  gave complementary information about the structure of LDH during the freeze—thaw process.

# Characterization of Deuterated NaP Buffer Solutions.

The phase behavior of aqueous phosphate buffer solutions of different concentrations, following freezing and thawing, has been reported in the literature. 6,42 Therefore, our current work was restricted to characterization of NaP buffer systems (10 and 100 mM) in 100% D<sub>2</sub>O. When NaP buffer solution (100 mM in  $D_2O$ ; pH of 7.0 at 25 °C) was cooled to -20 °C, the pH decreased to 4.1. Thus, a pH shift of 3.9 ( $\pm 0.7$ ; n = 3) units was observed (Figure 4A). The magnitude was similar to that observed in H<sub>2</sub>O solutions. The pH shift was attributed to selective crystallization of disodium hydrogen phosphate dodecahydrate (Na<sub>2</sub>HPO<sub>4</sub>·12H<sub>2</sub>O).<sup>7,42</sup> On cooling, peak characteristics of the dodecahydrate along with ice (ice I, D<sub>2</sub>O) were first observed at -10 °C in the XRD patterns (Figure 4C). The buffer salt peak intensities increased as the sample was cooled further to  $-40\,^{\circ}\text{C}$ . During heating, as the temperature of the sample increased from -40 to 10 °C, the dodecahydrate peaks persisted until 1 °C, whereas the ice peak intensity gradually decreased starting at -5 °C and vanished at 5 °C (Figure 4D). We believe that there is an overlapping of the eutectic (dodecahydrate-ice) and ice melting. The results can be explained by the higher melting temperature (+3.4 °C) of ice I (D<sub>2</sub>O) which was evident from DSC (Figure 4B).

On cooling a buffer solution of a lower concentration (10 mM), the pH shift was 3.3 ( $\pm 0.1$ ; n = 3) (Figure S6A). Thus, reducing the buffer concentration resulted in a lower pH shift. As before, from low-temperature XRD studies, selective crystallization of the dodecahydrate was evident during cooling (Figure S6C). The behavior of the system was substantially

similar to that observed at the higher buffer concentration (Figure S6B,D).

Freeze-Thaw of LDH in NaP Buffers. LDH buffered in NaP (10 and 100 mM) was subjected to freezing and thawing and the SANS curves were collected at select temperatures. At the higher buffer concentration, during cooling (Figure 5A), no changes in the SANS curves were observed at 20, 5, 0, and -10 °C, suggesting the retention of protein in the native state. At -25 and -45 °C, we see a gradual increase in intensity at LQS, indicative of tetramer aggregation. Above, we reported simultaneous ice and buffer salt crystallization at −10 °C based on XRD. The selective buffer salt crystallization led to a pH shift of ~3.9 units (low-temperature pH measurement). The tetramer aggregation may be attributed to one or more of the following factors: (i) ice crystallization leading to interfacial stress, (ii) freeze concentration, also a consequence of ice crystallization, and (iii) pH shift due to selective buffer crystallization. During warming of the frozen solution (Figure 5B), from -45 to 0 °C, the aggregation was retained. Even at 0 °C, ice melting was not complete and aggregation persisted (this was explained earlier in the context of Figure 2B). At 5 and 20 °C, even though the ice melting was complete, aggregation was evident, although it was much lesspronounced than at the lower temperatures. At 20 °C, some of the aggregates were retained. These post-thawing results were similar to that in histidine buffer except that there was more residual scattering in the LQS for LDH in histidine

A similar set of experiments were carried out for LDH solutions in 10 mM NaP buffer (Figure 5, panels C and D). We had earlier observed that freezing the buffer solution resulted in a pH shift of 3.3 units (Figure S6). This was lower than the shift of 3.9 units observed when a 100 mM phosphate buffer solution was cooled (Figure 4). The aggregation after freeze-thawing was about the same in the two systems (Figure 6). These results suggest that the magnitude of pH shift as well

as the buffer concentration did not have a discernible effect on the protein aggregation behavior.

We had earlier pointed out the potential for LDH aggregation in frozen histidine buffer solutions due to charge-charge interactions. In the phosphate-buffered systems, the buffer salt crystallization will shift the pH to the acidic range. The magnitude of shift is expected to be higher at 100 mM buffer concentration (Figures 4 and S6). It is now instructive to compare the net charge on LDH molecules in the two buffer systems. In the context of histidine buffer, we had pointed out that when the pH of the solution is 6.0 units, the calculated net positive charge on LDH was 10 units. The frozen phosphate-buffered systems are expected to be much more acidic. If the pH is reduced to 5, the net positive charge on the protein is 15 units, while at pH 4, it will be 20 units. Thus, the net positive charge in frozen LDH-buffered solutions (histidine or phosphate) is expected to be in the order of increasing pH: phosphate (100 mM) > phosphate (10 mM) > histidine. Interestingly, the consequence of the potential differences in protein surface charge could not be convincingly discerned using SANS (Figures 3 and 6).

Concentration Dependence of LDH Aggregation. LDH in solution, irrespective of the buffer used, aggregated on freezing. The aggregation was almost completely reversed on thawing. There appeared to be a small effect depending on the buffer used (perhaps more residual scattering from aggregates in histidine vs NaP), but there is no discernible effect on the buffer concentration (10 and 100 mM) for the NaP buffers. The SANS studies necessitated a protein concentration of 1000  $\mu$ g/mL so as to discern the conformation during different stages of freezing and thawing. We had earlier stated that LDH aggregated in freeze-thawed solutions when the LDH concentration was typically  $\leq 100 \ \mu g/$ mL.<sup>20-23</sup> This apparent difference in behavior could be attributed to the relatively high protein concentration in the SANS experiments leading to self-stabilization. In addition, the SANS results are based on a single freeze-thaw cycle. While it would be highly desirable to conduct multiple freeze-thaw cycles, this was not possible because of the limited availability of the beam time. It is noteworthy that each freeze-thaw cycle was 22 h long and only two samples were measured during that time.

The aggregation behavior in protein solutions of much lower concentrations ( $\sim 10~\mu g/mL$ ) can be evaluated by DLS. An added advantage of this technique is the extremely short analysis time of  $\sim 10~s$ . Solutions subjected to multiple freeze—thaw cycling could be immediately analyzed after thawing. This technique was therefore an excellent complement to SANS. Hence, the two limitations of the SANS technique, inability to analyze solutions with low protein concentration and evaluating the effect of multiple freeze—thaw cycles, were overcome using DLS.

The LDH protein solutions subjected to five freeze—thaw cycles and analyzed before and after freezing. The results are presented in Table 2. The key parameter of interest is the Z-average diameter, which is the intensity-weighted mean hydrodynamic size of the ensemble collection of particles. When buffered either with histidine or phosphate, irrespective of the starting LDH concentration, the hydrodynamic diameter is ~7 nm. This suggests that LDH exists as a tetramer in a monodisperse state, consistent with the SANS and SAXS results in Table 1. Dilute monodispersed solutions are a prerequisite for SANS/SAXS data. <sup>14</sup> In histidine buffer, at 10

Table 2. Particle Size of LDH in Solution before Freezing and after Five Freeze-Thaw Cycles<sup>a</sup>

		Z-avg diameter (nm) from DLS			
	buffer	LDH concentration $(\mu g/mL)$	control	5× FT	
a	10 mM histidine	10	6.3	291.3	
a	10 mivi mstidile	10	9.5	156.0	
			5.8	155.0	
		100	7.7	21.2	
		100	8.2	7.4	
			9.9	22.2	
		1000	8.0	9.0	
		1000	8.0	11.3	
			7.9	8.7	
ь	10 mM NaP	10	8.0	771.0	
-			9.5	>1000	
			6.3	272.0	
		100	7.5	116.0	
			8.2	>1000	
			9.9	>1000	
		1000	8.0	8.6	
			7.9	8.7	
			8.0	8.2	
c	100 mM NaP	10	5.0	>1000	
			12.9	>1000	
			16.9	>1000	
		100	7.9	>1000	
			7.3	>1000	
			8.1	>1000	
		1000	8.4	>772.8	
			8.3	>1000	
			8.0	>1000	

"The LDH concentrations were (i) 10, (ii) 100, and (iii) 1000  $\mu$ g/mL in three different buffer solutions (a) 10 mM histidine, (b) 10 mM NaP, and (c) 100 mM NaP. The freezing and thawing was carried out five times, and the runs were carried out for three aliquots, while the individual runs were an average of five scans. The three values were not averaged since the number of particles was not necessarily the same in the three aliquots.

 $\mu g/mL$  LDH concentration, there is a discernible increase in diameter after five freeze—thaw cycles, suggesting aggregation. Interestingly, at higher LDH concentrations (100 and 1000  $\mu g/mL$ ), the increase in diameter is much less-pronounced. At an LDH concentration of 1000  $\mu g/mL$ , even after five freeze—thaw cycles, there appears very little, if any, increase in diameter. Thus, by combining the SANS and DLS results for LDH at 1000  $\mu g/mL$ , we see evidence of aggregation in the frozen state with nearly complete reversibility (self-stabilization) after both one and five freeze—thaw cycles.

When the NaP buffer is at a low concentration (10 mM), after five freeze—thaw cycles, the Z-average diameter is substantially increased at a low protein concentration (10  $\mu$ g/mL). The observed diameter is higher than that observed in the histidine system. One possible explanation is the additional stress induced by buffer salt crystallization and the attendant pH shift. As the protein concentration is increased, first to 100 and then to 1000  $\mu$ g/mL, it is progressively more effective in inhibiting buffer salt crystallization. The consequence of this inhibition is the lower diameter after the freeze—thaw cycling with the high protein concentration (1000  $\mu$ g/mL) resulting in almost the same diameter as the control.

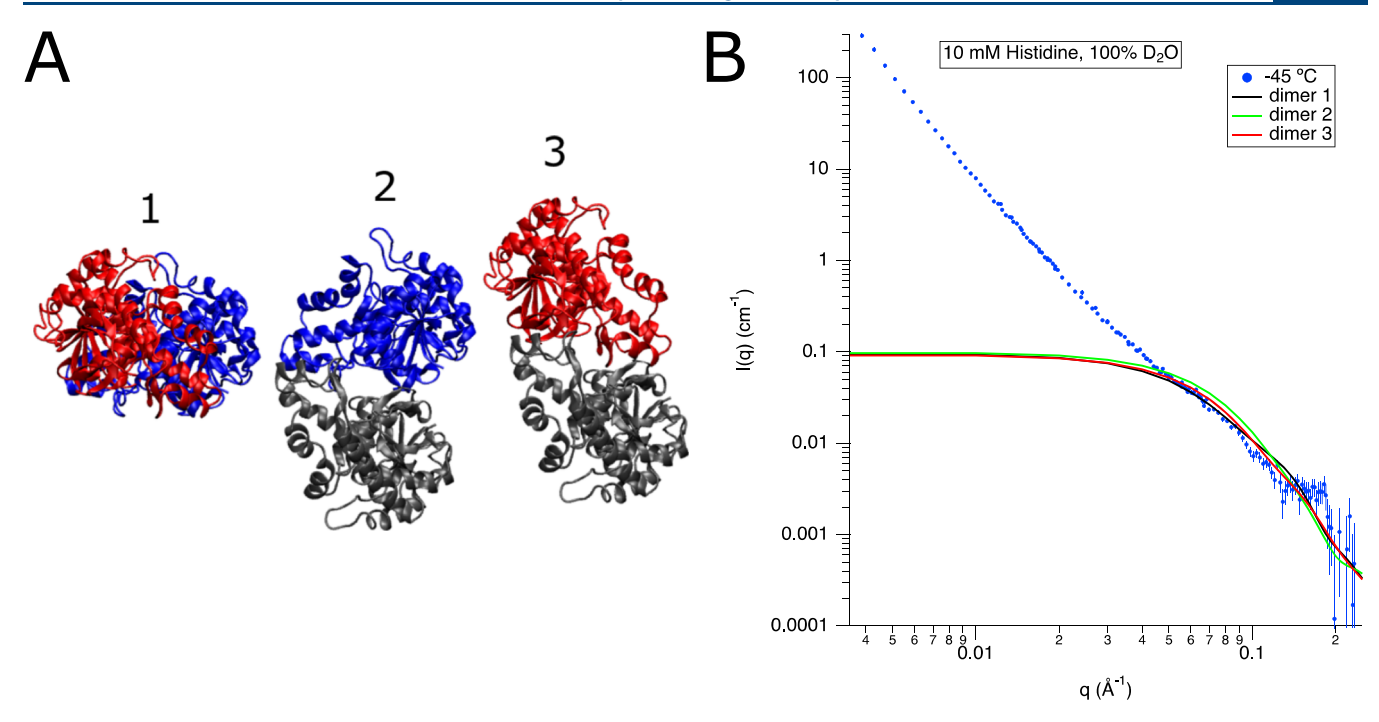


Figure 7. Modeling LDH dimers to determine the type of aggregates observed experimentally in 10 mM histidine buffer (100%  $D_2O$ ) solutions. (A) LDH dimers in three different forms, modeled as per Fujisawa et al. (B) Overlay of SANS curves for 1 mg/mL LDH in 10 mM histidine buffer in 100%  $D_2O$  (blue data points) at -45 °C and the reference LDH dimer 1, 2, and 3 curves (black, red, and green curves, respectively). Error bars are the standard error of the mean based on the number of pixels used during data averaging.

This is consistent with the SANS results after one freeze—thaw cycle.

At a high buffer concentration of 100 mM, there was pronounced aggregation up to a protein concentration of 100  $\mu$ g/mL. This result could be explained by the inability of the protein to prevent the pH shift upon freezing. Even at a protein concentration of 1000  $\mu$ g/mL, there is aggregation, although it is less pronounced than at lower protein concentrations. This suggests that although we did not see significant aggregation with SANS after one freeze-thaw cycle, aggregation was present after five cycles. This aggregation was not evident in the SAXS data (Figure S3) collected mainly in the HQS. However, the I(0) value in Table 1 is much lower than the calculated value after five freeze-thaw cycles, perhaps to be attributed to the loss of the sample due to air bubbles. In this case, it is more likely that the "loss" is due to a shift in the size distribution where the concentration of the tetramer is reduced as other populations of aggregates form. While these aggregates are not evident in the measured q range of the SAXS data, the I(0) value and the DLS results suggest that they are present.

Since both the SANS and DLS experiments were conducted at a protein concentration of 1000  $\mu$ g/mL, it is useful to compare them. At low buffer concentration (10 mM; histidine or NaP), there is no evidence of aggregation at RT after one freeze—thaw (SANS) or five freeze—thaw (DLS) cycles. Thus, solutions with high protein concentration coupled with low buffer concentration exhibited resistance to freezing and thawing stress. At a low protein concentration of 10  $\mu$ g/mL, irrespective of the buffer used, the stresses associated with the freeze—thaw cycling were sufficient to cause aggregation. Thus, the protein concentration appears to be a dominant factor when considering the stresses associated with freezing and thawing. In the case of proteins that are susceptible to

aggregation at low concentration, the use of additional excipients may offer a viable approach for stabilization.

**Modeling the Aggregates.** The dissociation of the LDH tetrameric structure and its stabilization due to factors such as temperature, pH, additives, and processing conditions (freeze—thaw and freeze-drying) have been a topic of several investigations.  $^{20,43-45}$  In an earlier gel chromatographic study performed at RT by Lovell and Winzor, LDH (2 mg/mL) was shown to dissociate from tetramer to dimer when the pH of solution was adjusted from pH 7 to 5 using acetate chloride. In addition, when exposed to pH 5, the conversion to LDH dimers was very rapid and the reaction was complete within a minute. Interestingly, when the solution pH was restored to pH 7, there was  $\sim$ 70% retention of activity. This was attributed to reversibility of the LDH dimers to the native tetrameric form. However, prolonged exposure of the dimers to pH 5 resulted in an increase in irreversible aggregation.  $^{43}$ 

LDH is known to self-stabilize at higher concentrations (>500  $\mu$ g/mL) during freeze-thawing and freeze-drying.<sup>20</sup> However, at lower LDH concentrations ( $\leq 500 \ \mu g/mL$ ), the reduction in activity recovery was reported in the presence of Na<sub>2</sub>HPO<sub>4</sub> salt formed as a result of a combination of NaCl with KPO<sub>4</sub>. The crystallization of Na<sub>2</sub>HPO<sub>4</sub> at low temperature was shown to cause an acidification effect leading to dissociation of the tetrameric structure into dimers. The pH shift  $(\Delta pH_{pH22^{\circ}C-(-20^{\circ}C)})$  in 10 mM KPO<sub>4</sub> and 0.1 M NaCl in the absence of LDH was 3 units. The addition of stabilizers such as BSA and PVP prevented LDH dissociation and resulted in maintenance of tetrameric LDH in the frozen state.<sup>20</sup> We believe that LDH exerts a self-stabilization effect which is concentration-dependent. The model SANS curves for LDH dimers were calculated (described in the Materials and Methods section). Figure 7A shows LDH dimers modeled as per Fujisawa et al. 33 The predicted SANS scattering of these

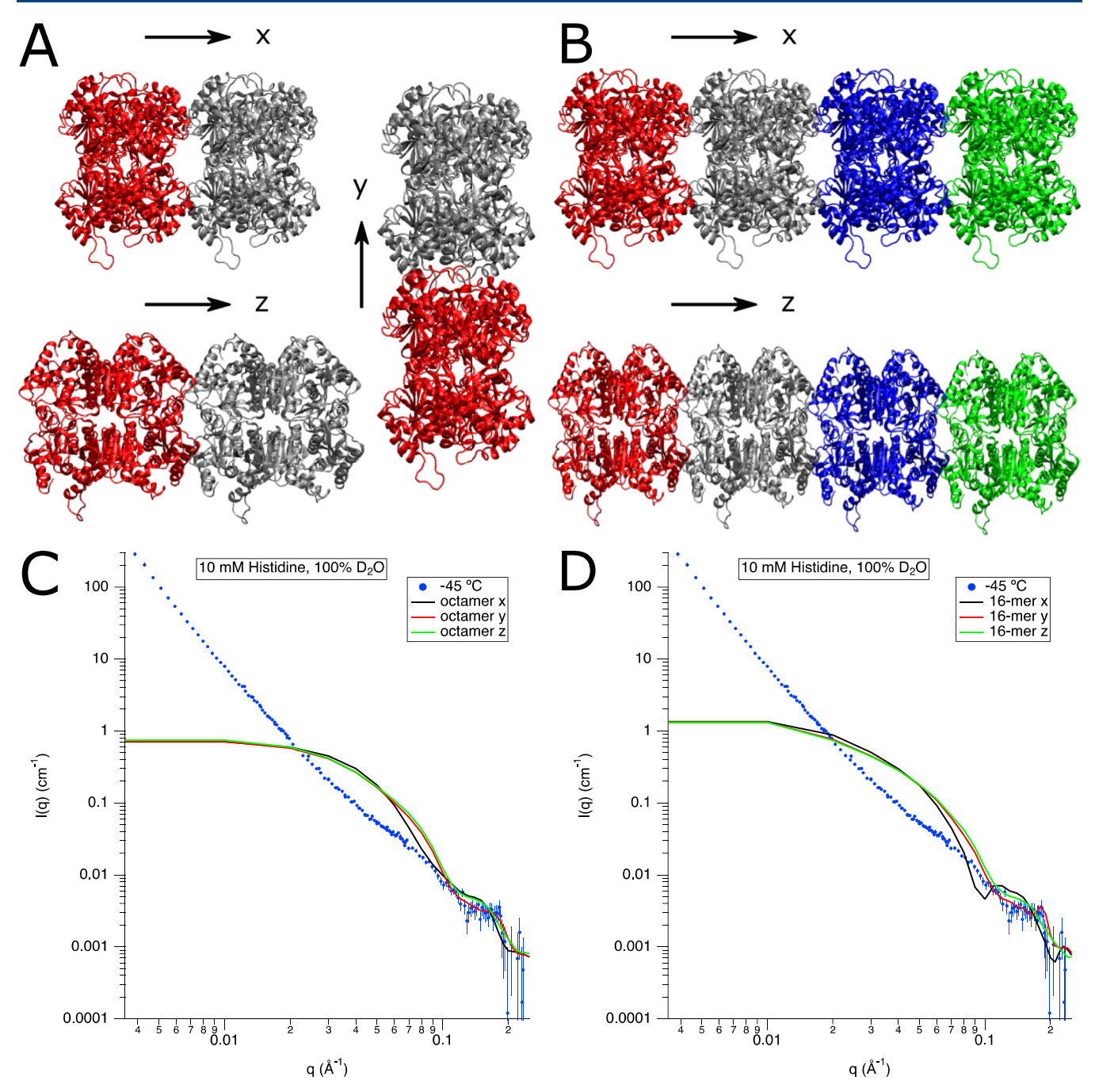


Figure 8. Modeling LDH aggregates to determine the type of aggregates observed experimentally in 10 mM histidine buffer ( $100\% D_2O$ ) solutions. (A) LDH octamers modeled in three different orientations. (B) LDH 16-mers modeled in three different orientations (y direction not shown). (C) Overlay of SANS curves for 1 mg/mL LDH in 10 mM histidine buffer in  $100\% D_2O$  (blue data points) at -45 °C and the reference LDH octamer curves in x, y, and z orientations (black, red, and green curves, respectively). (D) Overlay of SANS curves for 1 mg/mL LDH in 10 mM histidine buffer in  $100\% D_2O$  (blue data points) at -45 °C and the reference LDH 16-mer curves in x, y, and z orientations (black, red, and green curves, respectively). Error bars are the standard error of the mean based on the number of pixels used during data averaging.

dimers averaged over all possible orientations are overlaid with the SANS pattern from LDH (1000  $\mu g/mL$ ) in 10 mm histidine buffer (100%  $D_2O$ ) at -45 °C (frozen state, Figure 7B). The characteristic features of the modeled LDH dimers do not show any overlap with the experimental SANS pattern in the HQS for q>0.1 Å<sup>-1</sup> (we would not expect overlap at lower q values due to the difference in size between LDH dimers and the aggregates formed upon freezing).

These results were also consistent with SANS patterns obtained in the presence of NaP buffer (data not shown). As

mentioned earlier, we suggested that aggregates that form in the frozen state likely assemble from the tetramer. Thus, the native tetrameric structure is not lost upon freezing but rather becomes the building block for the higher-order aggregates. To probe this further, higher-order aggregates of the native tetramer were modeled including octamers (Figure 8A) and 16-mers (Figure 8B), and their respective SANS patterns were calculated (Figure 8C,D). These calculated patterns were overlaid with the SANS pattern from LDH (1000  $\mu$ g/mL) in 10 mm histidine buffer (100% D<sub>2</sub>O) at -45 °C. Comparing

SANS scattering in Figure 8C,D, at -45 °C, a pronounced deviation from the octamer and 16-mer structure is evident for the LQS scattering and a loss of signal is seen in the HQS between q = 0.025 and 0.1 Å<sup>-1</sup>. However, there is still some evidence of the subsidiary maximum at  $a = 0.15 \text{ Å}^{-1}$  which can be attributed to the native tetramer, the precursor for the formation of higher-order structures. Two important conclusions are (i) we did not observe the dissociation of the LDH tetramer into dimers in the presence of histidine or NaP buffer in the frozen state and (ii) the aggregates that formed in the frozen state were higher-order assemblies of the native tetrameric state (>16-mer). These higher-order LDH aggregates were almost completely reversible after a single freeze-thaw cycle in 10 mM histidine buffer and 10 or 100 mM NaP buffer solutions. The retention of the tetrameric state as the basic unit in the formation of higher-order aggregates was responsible for its reversibility post-thawing.

The abovementioned results were interesting given the fact that the LDH tetrameric structure did not dissociate into dimers and was reversible post-freeze-thawing at  $\sim 1000~\mu g/$  mL in both histidine and NaP buffer solutions, even in the absence of a stabilizing excipient such as a sugar or surfactant. The results are partly consistent with earlier observations from Anchordoquy et al., where they proposed a direct correlation between the maintenance of the LDH quaternary structure in the frozen state by stabilizers such as BSA and PVP and its activity recovery post-freeze-thawing and freeze-drying. <sup>20,44</sup> In comparison with earlier reports, wherein the behavior of LDH in the frozen state was followed by indirect studies and extrapolated from freeze—thaw studies, this is the first report where the conformation of LDH in the frozen state has been systematically evaluated using neutron scattering.

## SIGNIFICANCE

The stresses induced during freezing and thawing of protein solutions and their consequences on its stability are of immense interest to the pharmaceutical community. In most stress studies, the protein characterization is performed at the end of the freeze—thaw cycle and usually at RT. However, characterization in the frozen state is important for two reasons: (i) aggregation during freezing can be an intermediate or precursor to irreversible protein aggregation. Thus, aggregate characterization may aid in the development of mitigation strategies. (ii) If the aggregation is reversible on thawing, the reversibility kinetics is of practical importance.

In LDH solutions (1000  $\mu$ g/mL), irrespective of the buffer used (histidine or NaP), the aggregation observed in the frozen state was completely reversed when the solutions were thawed. The use of phosphate buffer provided an avenue to simultaneously evaluate the effects of stresses induced by freezing and pH shift. Phosphate buffer solutions are known to undergo pH shifts when frozen, and at high buffer concentration (100 mM), the pH shift can be very pronounced. At this buffer concentration, LDH aggregation was evident following multiple freeze-thaw cycling. However, aggregation was reduced when the buffer concentration was lowered to 10 mM (both histidine and phosphate). Interestingly, when the protein concentration was lowered (10 or 100  $\mu$ g/mL), the impact of the freezing stress was pronounced. These results suggest that the potential problems with the use of phosphate buffer may be overstated in the literature.

However, there was a limitation with the SANS studies. In order to get an adequate signal, the protein concentration used was  $1000~\mu g/mL$ . Proteins are known to be self-stabilizing at high concentrations. Protein solutions at much lower concentrations could be investigated by light scattering. Moreover, during long-term storage, a protein solution may undergo multiple freeze—thaw cycles. Therefore, the combined effects of low concentration and multiple freeze—thaw cycling were investigated by light scattering.

By combining SANS and DLS, comprehensive characterization was possible which could not have been accomplished with the individual techniques. At a protein concentration of  $1000~\mu g/mL$  (10~mM phosphate), SANS revealed self-association in the frozen state which was reversed on thawing. DLS confirmed the reversibility of the self-association even after five freeze—thaw cycles. However, DLS alone would not have revealed association of the native tetramer in the frozen state. While SANS provided qualitative information with respect to protein aggregation, the insights from DLS were quantitative with respect to the particle size of the aggregates.

Irrespective of the buffer used and the buffer concentration, there was evidence of aggregation when the LDH concentration was low (10  $\mu$ g/mL). However, when the protein concentration was higher ( $\geq$ 100  $\mu$ g/mL), only the high phosphate buffer concentration (100 mM) appeared to facilitate aggregation. Thus, the combined effects of potential pH shift and the repeated stress of freezing and thawing (five cycles) seem to be detrimental to protein stability.

### ASSOCIATED CONTENT

# **Supporting Information**

The Supporting Information is available free of charge at https://pubs.acs.org/doi/10.1021/acs.molpharmaceut.1c00666.

Guinier fits used to calculate  $R_{\rm g}$  and I(0); SAXS data; plot of LDH surface charge; low-temperature XRD, and low-temperature pH measurements (PDF)

# AUTHOR INFORMATION

# **Corresponding Authors**

Susan Krueger — Center for Neutron Research, National Institute of Standards and Technology, Gaithersburg, Maryland 20899, United States; Phone: 301-975-6734; Email: susan.krueger@nist.gov; Fax: 301-921-9847

Raj Suryanarayanan — Department of Pharmaceutics, College of Pharmacy, University of Minnesota, Minneapolis, Minnesota 55455, United States; ocid.org/0000-0002-6322-0575; Phone: (612) 624-9626; Email: surya001@umn.edu; Fax: (612) 626-2125

## **Authors**

Jayesh Sonje — Department of Pharmaceutics, College of Pharmacy, University of Minnesota, Minneapolis, Minnesota 55455, United States; Orcid.org/0000-0002-9893-6880 Seema Thakral — Department of Pharmaceutics, College of Pharmacy, University of Minnesota, Minneapolis, Minnesota 55455, United States; Characterization Facility, University of Minnesota, Minneapolis, Minnesota 55455, United States; Orcid.org/0000-0002-8044-5282

Complete contact information is available at: https://pubs.acs.org/10.1021/acs.molpharmaceut.1c00666

#### **Notes**

The authors declare no competing financial interest.

## ACKNOWLEDGMENTS

Certain commercial equipment, instruments, materials, suppliers, or software is identified in this paper to foster understanding. Such an identification does not imply recommendation or endorsement by the National Institute of Standards and Technology nor does it imply that the materials or equipment identified are necessarily the best available for the purpose. We acknowledge funding from the Kildsig Center for Pharmaceutical Processing Research and the William and Mildred Peters Endowment Fund. We thank Jason Hermann and Todd Geders from Bio-Techne, MN, for providing us access and generous help with the DLS studies. Parts of this work were carried out in the Characterization Facility, University of Minnesota, which receives partial support from the NSF through the MRSEC (award number DMR-2011401) and the NNCI (award number ECCS-2025124) programs.

### REFERENCES

- (1) Singh, S. K.; Kolhe, P.; Wang, W.; Nema, S. Large Scale Freezing of Biologics, A Practitioner's Review, Part One: Fundamental Aspects. *BioProcess Int.* **2009**, *7*, 32–44.
- (2) Chi, E. Y.; Krishnan, S.; Randolph, T. W.; Carpenter, J. F. Physical stability of proteins in aqueous solution: mechanism and driving forces in nonnative protein aggregation. *Pharm. Res.* **2003**, *20*, 1325–1336.
- (3) Thakral, S.; Sonje, J.; Munjal, B.; Suryanarayanan, R. Stabilizers and Their Interaction with Formulation Components in Frozen and Freeze-dried Protein Formulations. *Adv. Drug Delivery Rev.* **2021**, *173*, 1–19.
- (4) Singh, S. K.; Kolhe, P.; Mehta, A. P.; Chico, S. C.; Lary, A. L.; Huang, M. Frozen state storage instability of a monoclonal antibody: aggregation as a consequence of trehalose crystallization and protein unfolding. *Pharm. Res.* **2011**, *28*, 873–885.
- (5) Sundaramurthi, P.; Shalaev, E.; Suryanarayanan, R. "pH Swing" In Frozen Solutions Consequence of Sequential Crystallization of Buffer Components. *J. Phys. Chem. Lett.* **2010**, *1*, 265–268.
- (6) Gómez, G.; Pikal, M. J.; Rodríguez-Hornedo, N. Effect of initial buffer composition on pH changes during far-from-equilibrium freezing of sodium phosphate buffer solutions. *Pharm. Res.* **2001**, *18*, 90–97.
- (7) Thorat, A. A.; Munjal, B.; Geders, T. W.; Suryanarayanan, R. Freezing-induced protein aggregation Role of pH shift and potential mitigation strategies. *J. Controlled Release* **2020**, 323, 591–599.
- (8) Pikal-Cleland, K. A.; Carpenter, J. F. Lyophilization-induced protein denaturation in phosphate buffer systems: Monomeric and tetrameric  $\beta$ -galactosidase. *J. Pharm. Sci.* **2001**, *90*, 1255–1268.
- (9) Pikal-Cleland, K. A.; Rodríguez-Hornedo, N.; Amidon, G. L.; Carpenter, J. F. Protein denaturation during freezing and thawing in phosphate buffer systems: monomeric and tetrameric beta-galactosidase. *Arch. Biochem. Biophys.* **2000**, *384*, 398–406.
- (10) Duran, T.; Minatovicz, B.; Bai, J.; Shin, D.; Mohammadiarani, H.; Chaudhuri, B. Molecular Dynamics Simulation to Uncover the Mechanisms of Protein Instability During Freezing. *J. Pharm. Sci.* **2021**, *110*, 2457–2471.
- (11) Minatovicz, B.; Sun, L.; Foran, C.; Chaudhuri, B.; Tang, C.; Shameem, M. Freeze-concentration of solutes during bulk freezing and its impact on protein stability. *J. Drug Delivery Sci. Technol.* **2020**, 58, 101703.
- (12) Minatovicz, B.; Bogner, R.; Chaudhuri, B. Use of a Design of Experiments (DoE) Approach to Optimize Large-Scale Freeze-Thaw Process of Biologics. *AAPS PharmSciTech* **2021**, 22, 153.
- (13) Esfandiary, R.; Parupudi, A.; Casas-Finet, J.; Gadre, D.; Sathish, H. Mechanism of reversible self-association of a monoclonal antibody:

- role of electrostatic and hydrophobic interactions. *J. Pharm. Sci.* **2015**, 104, 577–586.
- (14) Jacques, D. A.; Trewhella, J. Small-angle scattering for structural biology—Expanding the frontier while avoiding the pitfalls. *Protein Sci.* **2010**, *19*, 642–657.
- (15) Curtis, J. E.; Nanda, H.; Khodadadi, S.; Cicerone, M.; Lee, H. J.; McAuley, A.; Krueger, S. Small-angle neutron scattering study of protein crowding in liquid and solid phases: lysozyme in aqueous solution, frozen solution, and carbohydrate powders. *J. Phys. Chem. B* **2012**, *116*, 9653–9667.
- (16) Khodadadi, S.; Clark, N. J.; McAuley, A.; Cristiglio, V.; Curtis, J. E.; Shalaev, E. Y.; Krueger, S. Influence of sorbitol on protein crowding in solution and freeze-concentrated phases. *Soft Matter* **2014**, *10*, 4056–4060.
- (17) Yearley, E. J.; Zarraga, I. E.; Shire, S. J.; Scherer, T. M.; Gokarn, Y.; Wagner, N. J.; Liu, Y. Small-angle neutron scattering characterization of monoclonal antibody conformations and interactions at high concentrations. *Biophys. J.* **2013**, *105*, 720–731.
- (18) Chilson, O. P.; Kitto, G. B.; Kaplan, N. O. Factors affecting the reversible dissociation of dehydrogenases. *Proc. Natl. Acad. Sci. U.S.A.* 1965, 53, 1006.
- (19) Vesell, E. S.; Yielding, K. L. Effects of pH, ionic strength, and metabolic intermediates on the rates of heat inactivation of lactate dehydrogenase isozymes. *Proc. Natl. Acad. Sci. U.S.A.* **1966**, *56*, 1317.
- (20) Anchordoquy, T. J.; Carpenter, J. F. Polymers protect lactate dehydrogenase during freeze-drying by inhibiting dissociation in the frozen state. *Arch. Biochem. Biophys.* **1996**, *332*, 231–238.
- (21) Bhatnagar, B. S.; Pikal, M. J.; Bogner, R. H. Study of the individual contributions of ice formation and freeze-concentration on isothermal stability of lactate dehydrogenase during freezing. *J. Pharm. Sci.* **2008**, *97*, 798–814.
- (22) Schwegman, J. J.; Carpenter, J. F.; Nail, S. L. Evidence of partial unfolding of proteins at the ice/freeze-concentrate interface by infrared microscopy. *J. Pharm. Sci.* **2009**, *98*, 3239–3246.
- (23) Fang, R.; Tanaka, K.; Mudhivarthi, V.; Bogner, R. H.; Pikal, M. J. Effect of controlled ice nucleation on stability of lactate dehydrogenase during freeze-drying. *J. Pharm. Sci.* **2018**, *107*, 824–830
- (24) Liao, X.; Krishnamurthy, R.; Suryanarayanan, R. Influence of the active pharmaceutical ingredient concentration on the physical state of mannitol—implications in freeze-drying. *Pharm. Res.* **2005**, 22, 1978–1985.
- (25) Gómez, G. Crystallization-related pH Changes during Freezing of Sodium Phosphate Buffer Solutions; University of Michigan, 1995.
- (26) Glinka, C. J.; Barker, J. G.; Hammouda, B.; Krueger, S.; Moyer, J. J.; Orts, W. J. The 30 m Small-Angle Neutron Scattering Instruments at the National Institute of Standards and Technology. *J. Appl. Crystallogr.* **1998**, *31*, 430–445.
- (27) Kline, S. R. Reduction and analysis of SANS and USANS data using IGOR Pro. *J. Appl. Crystallogr.* **2006**, *39*, 895–900.
- (28) Coquelle, N.; Fioravanti, E.; Weik, M.; Vellieux, F.; Madern, D. Activity, stability and structural studies of lactate dehydrogenases adapted to extreme thermal environments. *J. Mol. Biol.* **2007**, *374*, 547–562.
- (29) Phillips, J. C.; Braun, R.; Wang, W.; Gumbart, J.; Tajkhorshid, E.; Villa, E.; Chipot, C.; Skeel, R. D.; Kalé, L.; Schulten, K. Scalable molecular dynamics with NAMD. *J. Comput. Chem.* **2005**, 26, 1781–1802
- (30) Best, R. B.; Zhu, X.; Shim, J.; Lopes, P. E. M.; Mittal, J.; Feig, M.; MacKerell, A. D. Optimization of the Additive CHARMM All-Atom Protein Force Field Targeting Improved Sampling of the Backbone  $\phi$ ,  $\psi$  and Side-Chain  $\chi 1$  and  $\chi 2$  Dihedral Angles. *J. Chem. Theory Comput.* **2012**, *8*, 3257–3273.
- (31) Curtis, J. E.; Raghunandan, S.; Nanda, H.; Krueger, S. SASSIE: A program to study intrinsically disordered biological molecules and macromolecular ensembles using experimental scattering restraints. *Comput. Phys. Commun.* **2012**, *183*, 382–389.
- (32) Humphrey, W.; Dalke, A.; Schulten, K. VMD: Visual molecular dynamics. J. Mol. Graphics 1996, 14, 33–38.

- (33) Fujisawa, T.; Kato, M.; Inoko, Y. Structural characterization of lactate dehydrogenase dissociation under high pressure studied by synchrotron high-pressure small-angle X-ray scattering. *Biochemistry* **1999**, 38, 6411–6418.
- (34) Watson, M. C.; Curtis, J. E. Rapid and accurate calculation of small-angle scattering profiles using the golden ratio. *J. Appl. Crystallogr.* **2013**, *46*, 1171–1177.
- (35) Sarachan, K. L.; Curtis, J. E.; Krueger, S. Small-angle scattering contrast calculator for protein and nucleic acid complexes in solution. *J. Appl. Crystallogr.* **2013**, *46*, 1889–1893.
- (36) Thorat, A. A.; Suryanarayanan, R. Characterization of phosphate buffered saline (PBS) in frozen State and after Freezedrying. *Pharm. Res.* **2019**, 36, 98.
- (37) Al-Hussein, A.; Gieseler, H. Investigation of histidine stabilizing effects on LDH during freeze-drying. *J. Pharm. Sci.* **2013**, *102*, 813–826
- (38) Kolhe, P.; Amend, E.; Singh, S. K. Impact of freezing on pH of buffered solutions and consequences for monoclonal antibody aggregation. *Biotechnol. Prog.* **2010**, *26*, 727–733.
- (39) Nick Pace, C.; Alston, R. W.; Shaw, K. L. Charge—charge interactions influence the denatured state ensemble and contribute to protein stability. *Protein Sci.* **2000**, *9*, 1395–1398.
- (40) Yadav, S.; Laue, T. M.; Kalonia, D. S.; Singh, S. N.; Shire, S. J. The influence of charge distribution on self-association and viscosity behavior of monoclonal antibody solutions. *Mol. Pharm.* **2012**, *9*, 791–802
- (41) Wang, W.; Roberts, C. J. Protein aggregation Mechanisms, detection, and control. *Int. J. Pharm.* **2018**, *550*, 251–268.
- (42) Varshney, D. B.; Kumar, S.; Shalaev, E. Y.; Kang, S.-W.; Gatlin, L. A.; Suryanarayanan, R. Solute crystallization in frozen systems—use of synchrotron radiation to improve sensitivity. *Pharm. Res.* **2006**, 23, 2368–2374.
- (43) Lovell, S. J.; Winzor, D. J. Effects of phosphate on the dissociation and enzymic stability of rabbit muscle lactate dehydrogenase. *Biochemistry* **1974**, *13*, 3527–3531.
- (44) Anchordoquy, T. J.; Izutsu, K.-I.; Randolph, T. W.; Carpenter, J. F. Maintenance of quaternary structure in the frozen state stabilizes lactate dehydrogenase during freeze—drying. *Arch. Biochem. Biophys.* **2001**, *390*, 35–41.
- (45) Rudolph, R.; Jaenicke, R. Kinetics of reassociation and reactivation of pig-muscle lactic dehydrogenase after acid dissociation. *Eur. J. Biochem.* **1976**, 63, 409–417.